Thermal transport properties of defective graphene: A molecular dynamics investigation*

Yang Yu-Lin(杨宇霖)[a] and Lu Yu(卢 宇)[b)c)†]

[a] School of Opto-electronic and Communication Engineering, Xiamen University of Technology, Xiamen 361024, China
[b] College of Physics and Energy, Fujian Normal University, Fuzhou 350007, China
[c] Department of Information Technology, Concord University College, Fuzhou 350007, China

(Received 26 September 2013; revised manuscript received 10 April 2014; published online 10 August 2014)

In this work the thermal transport properties of graphene nanoribbons with randomly distributed vacancy defects are investigated by the reverse non-equilibrium molecular dynamics method. We find that the thermal conductivity of the graphene nanoribbons decreases as the defect coverage increases and is saturated in a high defect ratio range. Further analysis reveals a strong mismatch in the phonon spectrum between the unsaturated carbon atoms in 2-fold coordination around the defects and the saturated carbon atoms in 3-fold coordination, which induces high interfacial thermal resistance in defective graphene and suppresses the thermal conductivity. The defects induce a complicated bonding transform from sp^2 to hybrid sp–sp^2 network and trigger vibration mode density redistribution, by which the phonon spectrum conversion and strong phonon scattering at defect sites are explained. These results shed new light on the understanding of the thermal transport behavior of graphene-based nanomaterials with new structural configurations and pave the way for future designs of thermal management phononic devices.

Keywords: thermal conductivity, vacancy defect, graphene, molecular dynamics simulation

PACS: 65.80.Ck, 63.22.Rc, 63.20.kp, 31.15.xv **DOI:** 10.1088/1674-1056/23/10/106501

1. Introduction

Over the past decade, graphene-based nanomaterials have attracted much attention in the scientific community due to the excellent electrical, thermal, and mechanical properties that graphene sheets were predicted to have.[1–4] In nanoelectronic applications, as devices continue to shrink and circuit density increases, high thermal conductivity, which is essential for heat dissipation and electronics' cooling, plays an increasingly important role in device reliability.[5–8] Graphene is known to have the highest thermal conductivity (κ) ever reported, yet a wide scattering of experimental data ranging from 600 W/m·K to 5300 W/m·K[9–14] can be found in the literature. The main source of this discrepancy is often ascribed to the experimental techniques (suspended or supported). Due to solid nanoscale roughness, the disconformity between graphene and the underlying solid causes phonons to leak, thereby reducing the κ value of supported graphene relative to that of the suspended graphene.[10] Moreover, due to the long room temperature (RT) phonon mean free path ($\sim$ 750 nm[15]), κ is strongly dependent on sample size. Other differences, such as sample morphologies (monolayer/bilayer, etc.), can also induce variations in the measured value of κ. In addition to the experimental studies, substantial theoretical effort has been made to investigate the thermal transport behaviors of both graphene sheets and nanoribbons.[4,16–20] The calculations confirm the experimentally predicted high value of κ and support the observed effects of size and chirality on heat transport.[21] Additionally, structural imperfections, such as strains,[20] grain boundaries,[22] nanojunctions,[4] etc., are observed to seriously deteriorate the thermal transport.

In spite of much effort devoted to the thermal transport investigations in graphene, the effects of intrinsic defects (vacancies, topological defects, etc.) on κ have been seldom studied as of yet. Due to the second law of thermodynamics, uncertainties and imperfections in manufacturing process, defects are usually unavoidable in an experimentally produced sample. In most of the application situations, these defects can affect the material performance, with the influence being more or less significant for different defect types, defect concentrations, and chiralities. In the point-defect situation, random occurrence of vacancies and Stone–Wales (SW) defects were observed to filter intermediate and high frequency phonons by scattering. As high as 80% reduction in thermal conductivity was observed for a graphene sheet with 0.1% vacancies or 0.23% SW defects,[23] which reasonably explains the large difference in the value of κ between experimental measurement and theoretical calculation. In the line-defect situation, the experimentally synthesized polycrystalline graphene was found to possess high thermal resistance at the grain boundary.[22]

*Project supported by the National Natural Science Foundation of China (Grant No. 51202032), the National Key Project for Basic Research of China (Grant No. 2011CBA00200), the Natural Science Foundation of Fujian Province, China (Grant Nos. 2012J01004 and 2013J01009), and the Funds from the Fujian Provincial Education Bureau, China (Grant No. GA12064).

†Corresponding author. E-mail: fzluyu@163.com

© 2014 Chinese Physical Society and IOP Publishing Ltd

While the occurrence of defects reduces the thermal transport efficiency of graphene, the deviation from perfection can also be tolerant and be carefully engineered to achieve new functionalities. Through chemical functionalization, the defect-induced interlayer cross-links provide a stable platform for vertical alignment of multilayer graphene sheets; the thus-constructed three-dimensional thermal interfacial material was found to possess high in-plane thermal conductivity and low contact thermal resistance.[24] Periodic patterned functional groups were found to reduce the phonon lifetime and raise the group velocity of graphene sheet, thus achieving an ultra-low thermal conductivity without destroying the lattice for electronic conductance,[25] which is especially attractive in thermoelectric applications. For single-wall CNT with dense random point defects, κ was observed to converge to ~ 150 W/m·K;[26] phonon engineering can be easily achieved by controlling the defect concentration. The strong phonon scattering at the edge and at nanojunctions is often utilized to construct asymmetric heat conductance, thus obtaining thermal rectification in various graphene- and CNT-based nanostructures.[4,17]

In engineering applications, it would be beneficial if the thermal properties of graphene can be manipulated according to the demands. Although the influence of sparse defects on κ has been studied,[23] the effect of defect coverage and the underlying structure-performance relations have not so far been examined in detail. In this article, we focus on vacancy defects and perform molecular dynamics (MD) simulations to investigate the thermal transport properties of defective graphene nanoribbons with different incipient defect concentrations. Furthermore, the complicated interplays among defect coverage, bonding network, and phonon scattering, and their effects on heat conductance are examined.

2. Models and methods

2.1. Models

For convenience, we investigate a series of zigzag graphene nanoribbons with a size of 200 Å $\times$ 50 Å. Although the size is not large enough to reproduce the experimentally measured thermal conductivity of graphene, various previous investigations have revealed that this size is enough to reveal the heat conductance trend of graphene-based materials.[4,20] Vacancy defects are generated by removing atoms from the graphene sheet plane. The incipient defects are randomly distributed on the graphene basal planes according to a prescribed defect coverage ϕ (defined as $A_{\text{defect}}/A_{\text{total}} \times 100$, where A_{defect} and A_{total} are the in-plane area of defects and area of the pristine graphene). The random generation of the defect sites is carefully examined and the result shows no significant overlap with each other, thereby avoiding the large-sized defects and enabling a homogeneous distribution. In the low ϕ situation, a single vacancy (SV) defect is dominant. With increasing ϕ, increasing numbers of double vacancies (DVs) appear (see illustrations in Fig. 1). The maximum concentrations are limited to avoid the extensive appearance of high-order vacancy clusters, such as tri- and tetra-vacancies.

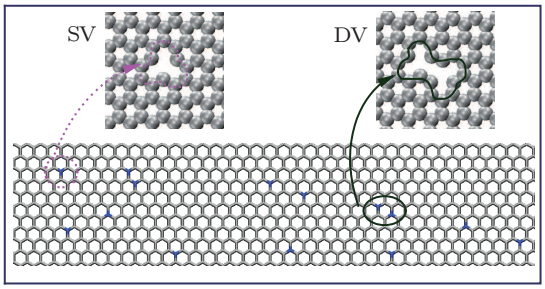


Fig. 1. (color online) Schematic illustrations of the zigzag graphene nanoribbon with vacancy defects. The vacancy defects are highlighted. The dominant defect type is single vacancy defect as demonstrated in the upper-left snapshot, where the edge of the defect is highlighted by dot curves. With increasing the defect coverage some of the single vacancies accumulate to form double vacancy defects as demonstrated in the upper-right picture, where the edge of the defect is highlighted by solid line curves.

2.2. Computational methods

Molecular dynamics (MD) simulations are performed using the massively parallelized modeling code lammps software package,[27] and the atomic interactions are described by the AIREBO potential.[28] Periodic boundary conditions are applied to the x and y axes. The velocity–verlet integration time step is set to be 0.5 fs. Structural optimizations are performed using the Polak–Ribière version of the conjugated gradient algorithm.[29] The MD simulations are performed with a background temperature of 300 K (Nosé–Hoover thermo bath,[30] coupling time constant 0.1 ps). After the equilibrium states are achieved in 200 ps, Microcanonical (NVE) ensembles are adopted and the reverse non-equilibrium molecular dynamics (RNEMD) method is used[31] to calculate the thermal conductivity. In this method, the investigated system is partitioned into 50 thin slabs of equal thickness along the heat transfer direction. Subsequently, the first slab at the boundary is assigned to be the "cold" slab (heat sink) and the 26th one is the "hot" slab (heat source). Then, a heat flux (energy flow rate, in units of W) is imposed by transferring energy from the heat sink to the heat source to form a temperature gradient (see lower inset in Fig. 2). In the Müller–Plathe nonequilibrium simulation, the heat flux J is injected/retrieved through momentum exchanges between the "hottest" atom (with kinetic energy $mv_{\text{h}}^2/2$) in the heat sink and the "coldest" atom (with kinetic energy $mv_{\text{c}}^2/2$) in the heat source. The momentum exchange is performed every 25 fs and the heat flux is collected during an interval of swap time t_{s}

$$J = \frac{\sum_{N_{\text{s}}} \frac{1}{2} m(v_h^2 - v_c^2)}{2t_{\text{s}}}, \tag{1}$$

where N_s is the number of swaps, m the atomic mass, v_h and v_c are the velocities of the hottest and coldest atoms in heat source and sink, respectively. After a 200-ps exchanging process, the nonequilibrium steady state can be achieved and the instantaneous kinetic energies of the atoms within each slab are averaged to evaluate the local temperature. The fluctuations are reduced by averaging events over a 100-ps time interval. With the temperature profile obtained, the temperature gradient $\partial T/\partial l$ can be computed and the thermal conductivity can be derived from the Fourier law approach by

$$\kappa = \frac{J/A}{\partial T/\partial l}, \tag{2}$$

where A is the cross section area at the heat transfer direction. The thickness of graphene is assumed to be 0.142 nm, which is the generally accepted C–C bond length.[32,33] We examine a zigzag graphene nanoribbon of 100 Å × 20 Å and find the thermal conductivity to be 78.1 W/m·K, which is consistent with the previous reports[4,33] and confirms the validity of the simulation methods used here. Although the thermal conductivity obtained by the RNEMD method is much smaller than the equilibrium Green–Kubo calculations[34] (which can yield the values much closer to the experimentally measured ones), the general trend predicted by the RNEMD calculations is the same and the nonlinearity can be avoided by using a small thermal gradient.

For the further analysis of the contributions to the thermal conductivity, the phonon spectrum function $G(\omega)$ is calculated from the Fourier transform of the velocity autocorrelation function (VACF):[35]

$$G(\omega) = \frac{1}{\sqrt{2\pi}} \int_0^\infty \mathrm{e}^{\mathrm{j}\omega t} \left\langle \sum_i v_i(t+t_0) v_i(t_0) \right\rangle \mathrm{d}t, \tag{3}$$

where ω is the vibration wave number, and $v_i(t)$ the velocity of the atoms. The velocity is recorded every 1 fs and the averaging is performed over 50-ps time interval after the system has reached an equilibrium state.

3. Results and discussion

3.1. Temperature profile

First, we investigate the difference in general heat transfer between pristine and defective graphene. The steady energy transfer state is reached quickly after the momentum exchange process has begun, and cumulated heat flow increases linearly with the elapse of time. Figure 2 shows the plot of temperature profiles for a pristine graphene and a typical vacancy defective graphene. To avoid any bias in the time averaging of the temperature, we average the temperature across the bin when the temperature gradient profile is stable (after 2 ns). Due to the size effect and high thermal conductivity of graphene,[36] the temperature profile is nonlinear in the vicinity of the heat source and sink. Thus, we take the temperature gradient from the middle portion between the thermostats to avoid edge effects. In the pristine graphene situation, heat transfer is fast and near-equilibrium thermal transport is reached close to the thermostats, which are represented by sharp temperature drop/jump at the thermostat edge and ultralow temperature gradient within the middle portion (Fig. 2), thus enabling the ultrahigh thermal conductivity of the pristine graphene. In the presence of vacancy defects, the heat transfer rate is significantly reduced. The temperature drop/jump at the thermostat edge is noticeably smaller, and the separation between thermal bath and linear temperature gradient region is greatly enlarged (from ∼ 12 nm to ∼ 24 nm in this case). The reason for this lies in the frequent blocking of heat transfer at the defect site. Moreover, the increased temperature gradient between heat sources and sinks can also be predicted. From this point of view, reduced thermal conductivity can be expected in defective graphene.

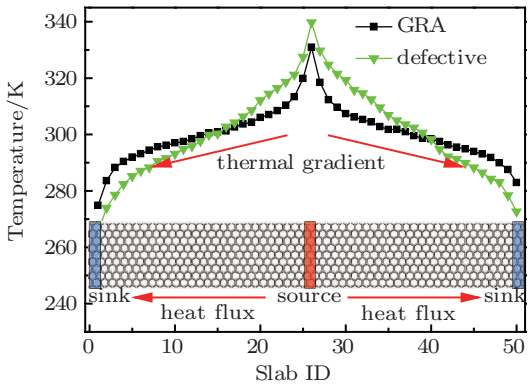


Fig. 2. (color online) Temperature profiles for a pristine graphene nanoribbon and a defective graphene nanoribbon. Both ribbon sizes are 200 Å × 50 Å. The lower inset is the schematic illustration of the thermostats. By momentum exchanging a heat flux is created between heat source and sinks, thus a thermal gradient can be obtained. The ribbon is partitioned into 50 thin slabs of equal thickness and the slab ID in the x axis corresponds to the index of the slabs.

One more phenomenon that should be noticed in Fig. 2 is that the middle portions of the temperature profiles are nearly linear. The presence of defects induces only small perturbations to the curve slope without sharp jump, as observed at the grain boundaries.[22] The temperature jump across the grain boundary is usually high, and the boundary conductance needs to be considered when discussing the thermal conductance. However, in the present situation, the vacancy defects are randomly distributed over the entire system, therefore producing a "homogeneous" defective system. The ensemble averaged effect of all the defects leads to a reduced heat transfer rate and a uniformly increased temperature slope, thus the thermal conductivity can still be calculated.

3.2. Thermal conductivities

Next, we study the effects of varying densities of vacancy defects on the lattice thermal transport properties of

graphene. The predominant defect type is SV, and with increasing the defect coverage more and more DVs appear (see Fig. 1). Higher order defects are seldom observed. Each defect is treated as an individual scattering center without considering the number of atoms that forms it. The thermal transport properties of pristine graphene are first calculated. The corresponding heat flux in the steady state is found to be 1.38 eV/ps and the obtained thermal conductivity is 172.91 W/m·K, which fall in the varying range for graphene and CNTs that were previously reported.[4,20,31] With the occurrence of defects, the heat flux is observed to drop almost linearly at first and then become saturated to ~ 1.15 eV/ps when $\phi > 7\%$ (corresponding to 17% reduction with respect to pristine graphene), as seen in Fig. 3(a). However, thermal conductivity is found to decrease nearly in parabolic manner in the low ϕ range. A rapid drop ($\sim 14\%$ reduction) is observed with the first few existing defects ($\phi = 0.2\%$). The lattice thermal conductivity converge to ~ 15.3 W/m·K when $\phi > 7\%$, corresponding to up to 90% suppression compared with its pristine thermal conductivity value. The quick decrease of κ can be understood from the strong reduction in the phonon mean free path. The total mean free path can be evaluated by $l_{\rm mfp}^{-1} = l_{\rm elastic}^{-1} + l_{\rm anharmonic}^{-1}$, thus it is determined by the shortest $l_{\rm anharmonic}$, which is dominated by the intrinsic defect scattering, even for low defect coverage. A similar trend was obtained by Hao *et al*. by using a combined MD simulation and an effective medium theory analysis.[37] Furthermore,

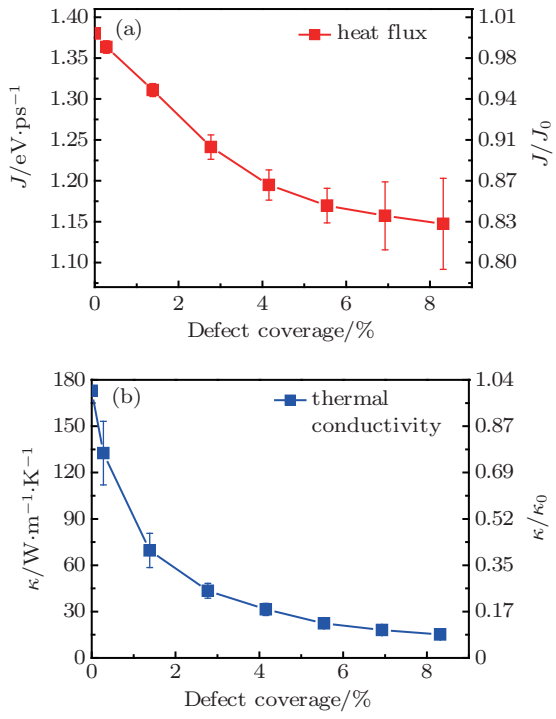


Fig. 3. (color online) Variations of (a) heat flux and (b) thermal conductivity with defect coverage. The normalized values J_0 and κ_0 are those of the pristine graphene, that is, 1.38 eV/ps and 172.9 W/m·K, respectively. The error bars represent the respective standard deviations calculated from the ten independent simulations.

they proposed a modified Maxwell–Garnett formula, which reveals that the sensitivity of κ to ϕ originates from the scattering of phonons by defects and their delocalized mutual interaction.

3.3. Phonon spectra and bond length analysis

Finally, to understand the underpinning mechanism of the defect effect on thermal transport properties, we investigate the phonon spectra of pristine and defective graphene (see Fig. 4). By recording the velocities of the atoms within the system, we obtain the VACF function as described above; thereafter, we calculate the phonon spectrum function $G(\omega)$ from its Fourier transform. $G(\omega)$ demonstrates the vibration energy with respect to vibration frequency, which is proportional to the product of phonon density of state and mode occupation number. From the structural configurations, as demonstrated in Fig. 1, one can see that the pristine graphene contains only one type of carbon atom in 3-fold coordination, while the defective graphene contains two types of carbon atoms, that is, minority carbon atoms in 2-fold coordination around the defect sites and majority carbon atoms in 3-fold coordination elsewhere. In order to distinguish the distinctive contributions of these atoms, we define carbon atoms in 2-fold coordination as type "C_2" and 3-fold coordination as type "C_3" and calculate the phonon spectra for all these types of atoms. Figure 4(a) demonstrates the phonon spectrum of the pristine graphene and the characteristic G band (~ 52 THz) of monolayer graphene. This peak manifests itself in the defective graphene (Figs. 4(b) and 4(c)), showing that the vibration modes for the majority C_3 atoms are well preserved. However, the peak intensity is remarkably suppressed with increasing defect coverage ϕ, resulting in broadened peaks and smoothed phonon spectrum. There is a strong suppression of higher frequency modes, and generally low frequency modes are enhanced under disorder. More interestingly, we find that the relative intensities in a range of 0 THz $\sim$ 5 THz are significantly enlarged. To understand the origin of the unusual enhancement, we calculate the phonon spectra of C_2 atoms for low and high defect coverage ($\phi = 0.2\%$ and 8.2%, respectively). From the obtained results, as presented in Figs. 4(d) and 4(e), one can see that the G band is shifted towards the higher frequency range (~ 56 THz) and suppressed intensity increases. The characteristic peak for C_2 atoms is no longer in the G band but lies in a low frequency range (~ 2.5 THz). The low frequency wave modes are conducted almost perfectly among C_2 atoms, while high frequency wave modes are suppressed remarkably. The strong mismatch between the phonon spectra for C_2 and C_3 atoms shows low thermal transport efficiency across C_2/C_3 interface, which is corresponding to the generally accepted explanation of strong phonon scattering at the defect site. The strong interface mismatch causes the phonon

mean free path to decrease and the thermal conductivity to degrade since $\kappa = \sum_m C_v v_m l_{\rm mfp}$, where C_v, v_m, and $l_{\rm mfp}$ are specific heat, group velocity, and phonon mean free path length, respectively. From the above investigation, we can conclude that the occurrence of C_2 atoms induces large interfacial thermal resistance and slows down the heat transfer, leading to a reduced thermal conductivity.

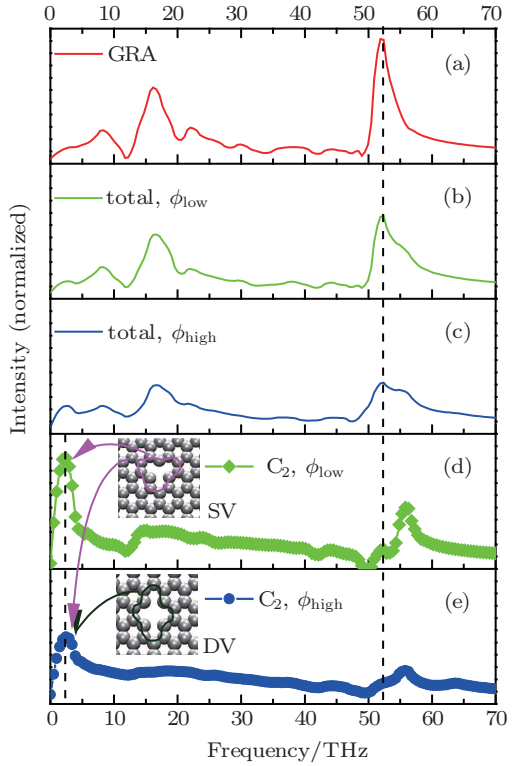


Fig. 4. (color online) Phonon spectra of pristine and defective graphene nanoribbons. (a) Pristine graphene containing C_3 atoms, and characteristic G band; (b) defective graphene with $\phi = 0.2\%$, containing both C_2 and C_3 atoms; (c) defective graphene with $\phi = 8.2\%$, containing both C_2 and C_3 atoms; (d) phonon spectrum for the C_2 atoms in lightly defective graphene ($\phi = 0.2\%$); (e) phonon spectrum for the C_2 atoms in highly defective graphene ($\phi = 8.2\%$).

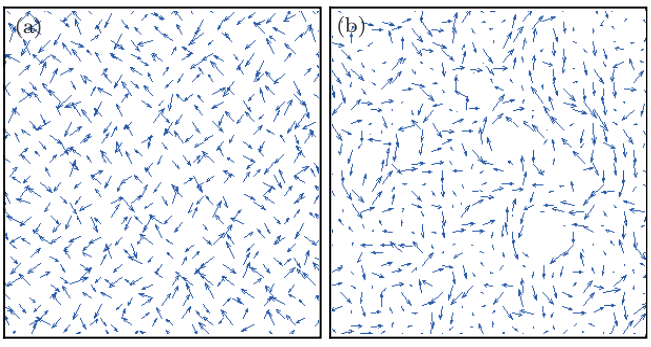


Fig. 5. (color online) Microscopic heat flux distributions on (a) pristine graphene and (b) defective graphene. The plotting regions are selected from the center of the sheet to avoid the edge effect.

To obtain an insight into this phenomenon, we calculate the microscopic flux for a pristine graphene and a defective graphene by using an equilibrium molecular dynamics (EMD) method. The system is subject to a microcanonical ensemble at background temperature of 300 K (Nosé–Hoover thermostat). Heat flux J is defined as $J = \left(\sum_i e_i v_i - \sum_i S_i v_i\right)/V$, where $\boldsymbol{e}$, $\boldsymbol{v}$, and $\boldsymbol{S}$ are the atomic energy, velocity vector, and stress tensor, respectively. From a comparison between Figs. 5(a) and 5(b), it follows that the distribution of microscopic heat flux is uniform on a pristine graphene sheet but complicated on a defective graphene sheet. Significant scattering occurs around the defects, leading to highly dispersive heat conduction.

Furthermore, from the comparison between Figs. 4(d) and 4(e) we see that the defect coverage also plays an important role in changing the shape of the phonon spectrum. In the low defect coverage situation, C_2 atoms from SV defect give rise to sharp peak at 2.5 THz (Fig. 4(d)), whereas in the high defect coverage circumstance the combined effects of C_2 atoms from both SV and DV defects suppress the peak intensity remarkably (Fig. 4(e)). To shed light on this phenomenon, we present in Fig. 6 the variations of the average bond length defect coverage, respectively, for ensemble averaged atoms, C_2 atoms, and C_3 atoms. Herein, the bond average is taken among all the bonds connected to the objective atom. For C_2 atoms, there are two bonds connected to each atom and the average is taken first between each pair of bonds and then among all of the C_2 atoms. The same rule extends to C_3 atoms, except that they are a 3-fold coordination. Finally, the ensemble averaged bondlength is calculated from all of the atoms within the investigated system. Interestingly, we find that the averaged $L_{\rm bond}$ for C_2 atoms decreases with ϕ increasing, whereas the L bonds for others enlarge. For the 3-fold coordination C_3 atoms, the interatomic bonds are always sp^2-hybridized. However, for the 2-fold coordination C_2 atoms the interatomic bonds become much more complicated. In the low ϕ range, SV is predominant and C_2 atoms are isolated (see lower-left inset in Fig. 6), the bonds connected to C_2 atoms are pseudo-sp^2-hybridized, therefore averaged $L_{\rm bond}$ approaches to 1.404 Å; that is, the value of the average sp^2 bondlength.[38,39] However, in the high ϕ range the number of DV is significantly enlarged and some of the C_2 atoms link directly to each other through sp-hybridization (see lower-right inset in Fig. 6), thus forming a hybrid sp–sp^2 bonding network. The average $L_{\rm bond}$ decreases from 1.403 Å to 1.399 Å with ϕ increasing from 0.2% to 8.2%. Due to the contributions from sp^2-bonds, the obtained bondlengths are much larger than the sp bondlength of 1.34 Å, as predicted by the AIREBO potential,[40,41] and that of 1.19 Å, as predicted by the ReaxFF potential.[42] For the sp^2-bonds among C_3 atoms, as the the value of ϕ increases the interatomic bonding strength is degraded, thus the average $L_{\rm bond}$ enlarges from 1.404 Å to 1.408 Å within the investigated ϕ range. Bondlength increasing within sp^2-network has been previously reported to soften the phonon,[20] and the decreasing bondlength in C_2 atoms can lead to more hard-

ened modes and, therefore, more uniform distribution of total phonon density of states. It is the complicated sp–sp^2 bonding network in a high ϕ situation that leads to the reduced peak value and broadened peak shape near 2.5 THz. On the basis of the above discussion, it is evident that the transform to hybrid sp–sp^2 bonding network changes the characteristic peak in the phonon spectrum and the variance in bondlength triggers more vibrational modes, which finally changes the distribution of the phonon density of states.

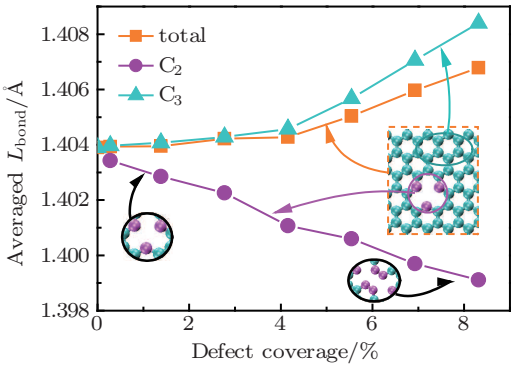


Fig. 6. (color online) Variations of averaged bond length with defect coverage for different types of carbon atoms within defective graphene nanoribbons. Results for ensemble averaged, C_2, and C_3 atoms are represented by solid square line, solid circle line, and solid triangle line, respectively.

4. Conclusions

In this work, we investigate, through molecular dynamics simulations, the thermal transport in graphene nanoribbons with randomly distributed vacancy defects. We demonstrate that small changes in defect coverage can lead to large reduction in thermal conductivity in low defect coverage range, and when the defect coverage rises above a certain value the thermal conductivity converges to a finite limit; that is, it is no longer sensitive to increasing disorder. The heat transfer rate shows a noticeable reduction near the thermal bath in the presence of structural defects, and the temperature gradient is significantly enlarged. The bonding configuration transforms from sp^2-network in pristine graphene to hybridized sp–sp^2-network in high defect coverage situation, and the interatomic bond length enlarges or shortens sinuously. Owing to this, strong phonon mismatches are observed at the C_2/C_3 interfaces, which gives rise to phonon scattering at defect sites, leading to reduced thermal conductivity. Our computations, as presented in this work, give a new insight into the defect and interface-induced thermal transport change, and may also help to improve the nanoengineering of heat transfer within graphene-based phonon devices.

References

[1] Novoselov K S, Geim A K, Morozov S V, Jiang D, Zhang Y, Dubonos S V, Grigorieva I V and Firsov A A 2004 *Science* **306** 666
[2] Zheng Y P, Wei N, Fan Z Y, Xu L Q and Huang Z G 2011 *Nanotechnology* **22** 405701
[3] Zheng Y, Xu L, Fan Z, Wei N, Lu Y and Huang Z 2012 *Current Nanoscience* **8** 89
[4] Xu L, Wei N, Zheng Y, Fan Z, Wang H and Zheng J 2012 *J. Mater. Chem.* **22** 1435
[5] Song J Q, Shi X, Zhang W Q and Chen L D 2013 *Physics* **42** 112 (in Chinese)
[6] Zhang G and Huang S Y 2013 *Physics* **42** 100 (in Chinese)
[7] Zhou J and Li B W 2013 *Physics* **42** 89 (in Chinese)
[8] Wu H Q, Linghu C Y, Lü H M and Qian H 2013 *Chin. Phys. B* **22** 098106
[9] Balandin A A, Ghosh S, Bao W, Calizo I, Teweldebrhan D, Miao F and Lau C N 2008 *Nano Lett.* **8** 902
[10] Seol J H, Jo I, Moore A L, Lindsay L, Aitken Z H, Pettes M T, Li X, Yao Z, Huang R, Broido D, *et al.* 2010 *Science* **328** 213
[11] Ghosh S, Bao W, Nika D L, Subrina S, Pokatilov E P, Lau C N and Balandin A A 2010 *Nat. Mater.* **9** 555
[12] Cai W, Moore A L, Zhu Y, Li X, Chen S, Shi L and Ruoff R S 2010 *Nano Lett.* **10** 1645
[13] Faugeras C, Faugeras B, Orlita M, Potemski M, Nair R R and Geim A K 2010 *ACS Nano* **4** 1889
[14] Pettes M T, Jo I, Yao Z and Shi L 2011 *Nano Lett.* **11** 1195
[15] Ghosh S, Calizo I, Teweldebrhan D, Pokatilov E P, Nika D L, Balandin A A, Bao W, Miao F and Lau C N 2008 *Appl. Phys. Lett.* **92** 151911
[16] Kong B D, Paul S, Nardelli M B and Kim K W 2009 *Phys. Rev. B* **80** 033406-4
[17] Hu J, Ruan X and Chen Y P 2009 *Nano Lett.* **9** 2730
[18] Evans W J, Hu L and Keblinski P 2010 *Appl. Phys. Lett.* **96** 203112-3
[19] Li W, Sevinçli H, Cuniberti G and Roche S 2010 *Phys. Rev. B* **82** 041410-4
[20] Wei N, Xu L, Wang H and Zheng J C 2011 *Nanotechnology* **22** 105705
[21] Balandin A A 2011 *Nat. Mater.* **10** 569
[22] Bagri A, Kim S P, Ruoff R S and Shenoy V B 2011 *Nano Lett.* **11** 3917
[23] Haskins J, Kinaci A, Sevik C, Sevinçli H, Cuniberti G and Çağin T 2011 *ACS Nano* **5** 3779
[24] Liang Q, Yao X, Wang W, Liu Y and Wong C P 2011 *ACS Nano* **5** 2392
[25] Kim J Y, Lee J H and Grossman J C 2012 *ACS Nano* **6** 9050
[26] Sevik C, Sevinçli H, Cuniberti G and Çağin T 2011 *Nano Lett.* **11** 4971
[27] Plimpton S 1995 *J. Comput. Phys.* **7** 1
[28] Brenner D W, Shenderova O A, Harrison J A, Stuart S J, Ni B and Sinnott S B 2002 *J. Phys.: Condens. Matter* **14** 783
[29] Polak E (ed.) 1997 *Optimization: Algorithms and Consistent Approximations* (New York: Springer)
[30] Hoover W G 1985 *Phys. Rev. A* **31** 1695
[31] Müller-Plathe F 1997 *J. Chem. Phys.* **106** 6082-5
[32] Zheng Y P, Xu L Q, Fan Z Y, Wei N and Huang Z G 2012 *J. Mater. Chem.* **22** 9798
[33] Xu Z P and Buehler M J 2009 *Nanotechnology* **20** 185701
[34] Wang Y L, Song Z G and Xu Z P 2013 *J. Mater. Res.* http://dx.doi.org/10.1557jmr.2013.380
[35] Alaghemandi M, Leroy F, Müller-Plathe F and Böhm M C 2010 *Phys. Rev. B* **81** 125410
[36] Schelling P K, Phillpot S R and Keblinski P 2002 *Phys. Rev. B* **65** 144306
[37] Hao F, Fang D and Xu Z 2011 *Appl. Phys. Lett.* **99** 041901
[38] Xu L Q, Wei N, Xu X M, Fan Z Y and Zheng Y P 2013 *J. Mater. Chem. A* **1** 2002
[39] Xu L Q, Wei N and Zheng Y P 2013 *Nanotechnology* **24** 505703
[40] Yang Y L and Xu X M 2012 *Comput. Mater. Sci.* **61** 83
[41] Zhang Y Y, Pei Q X and Wang C M 2012 *Comput. Mater. Sci.* **65** 406
[42] Cranford S W, Brommer D B and Buehler M J 2012 *Nanoscale* **4** 7797